



1    **Multi-Machine Learning Ensemble Regionalization of Hydrological**  
2    **Parameters for Enhances Flood Prediction in Ungauged Mountainous**  
3    **Catchments**

4  
5    Kai Li, Linmao Guo, Genxu Wang\*, Jihui Gao\*, Xiangyang Sun, Peng Huang,  
6    Jinlong Li, Jiapei Ma, Xinyu Zhang  
7  
8    *State Key Laboratory of Hydraulics and Mountain River Engineering, College of Water Resource*  
9    *and Hydropower, Sichuan University, Chengdu, 610000, China*  
10    \*Corresponding author: Genxu Wang (wanggx@scu.edu.cn) and Jihui Gao (jgao@scu.edu.cn).

11  
12    **Abstract:**

13        Machine learning-based parameter regionalization is an important method for  
14    flood prediction in ungauged mountainous catchments. However, single machine  
15    learning parameter regionalization often exhibits limitations in prediction accuracy and  
16    robustness. Therefore, this study proposes a multi-machine learning ensemble  
17    regionalization method that integrates Gradient Boosting Machine (GBM), K-Nearest  
18    Neighbors (KNN), and Extremely Randomized Trees (ERT) methods (GBM-KNN-  
19    ERT) to regionalize the sensitive parameters of the Topography-Based Subsurface  
20    Storm Flow (Top-SSF) model. Validated across 80 mountainous catchments in  
21    southwestern China, the GBM-KNN-ERT method demonstrates superior performance  
22    with 90% of ungauged catchments achieving the Nash-Sutcliffe Efficiency (NSE)  
23    above 0.9, representing a 67.44% improvement over single machine learning parameter  
24    regionalization. Notably, the GBM-KNN-ERT method shows improved robustness to  
25    climate change and changes in the number of donor catchments compared to other  
26    regionalization methods. An optimal balance between accuracy and computational



27 efficiency was achieved using 20-40 high quality donor catchments (NSE greater than  
28 0.85). This study provides systematic evidence that multi-machine learning ensemble  
29 can effectively address regionalization challenges in ungauged mountainous regions,  
30 offering a reliable tool for water resource management and flood disaster mitigation.

31 **Keywords:** Flood forecasting; Regionalization; Ungauged mountainous catchments;  
32 Top-SSF model;

33

34 **Highlights:**

- 35 1. Proposes a novel multi-machine learning ensemble regionalization method  
36 2. The GBM-KNN-ERT method demonstrate superior performance compared to other  
37 methods.  
38 3. The GBM-KNN-ERT method exhibits greater stability under climate change.

39



## 40        **1. Introduction**

41        Floods in mountainous catchments pose a significant threat to human safety and  
42        property, particularly in regions lacking sufficient observational data (Luo et al., 2015;  
43        Zhai et al., 2018). While hydrological models like the Topography-Based Subsurface  
44        Storm Flow (Top-SSF) mode (Li et al., 2024) offer promising simulation capabilities,  
45        their application in ungauged catchments is severely limited by the absence of  
46        calibration data (Choi et al., 2023; Liu et al., 2018). Effective parameter regionalization  
47        methods are therefore essential for transferring hydrological knowledge from gauged  
48        to ungauged regions, enabling reliable flood prediction in ungauged mountainous  
49        catchment (Garambois et al., 2015; Ragetti et al., 2017; Xu et al., 2018).

50        Parameter regionalization is a crucial method for flood prediction in ungauged  
51        catchments (Arsenault et al., 2022; Guo et al., 2021; Kratzert et al., 2019; Zhang et al.,  
52        2020). Compared to purely data-driven methods, parameter regionalization offers  
53        enhanced physical interpretability (Nearing et al., 2024; Tang et al., 2023; Zhang et al.,  
54        2024). Existing parameter regionalization methods can be broadly classified into three  
55        categories: similarity-based, hydrological signatures-based, and regression-based  
56        (Arsenault et al., 2019; Wu et al., 2022). Similarity-based methods rely on the  
57        assumption that catchments with similar characteristics exhibit similar hydrological  
58        responses, considering spatial proximity (Arsenault et al., 2019; Pugliese et al., 2018;  
59        Yang et al., 2018) and physical similarity (similar climatic and land cover conditions  
60        have similar hydrological characteristics) (Kanishka et al., 2017; Papageorgaki et al.,  
61        2016). The hydrological-signatures-based methods forms a regression relationship



62 between hydrological signatures (quantitative metrics that describe statistical or  
63 dynamic properties of streamflow) and catchment descriptors (McMillan, 2021; Zhang  
64 et al., 2018). Regression-based methods, which directly link hydrological model  
65 parameters to catchment descriptors, are widely used due to their simplicity and  
66 computational efficiency (Guo et al., 2021; Kratzert et al., 2019; Song et al., 2022; Wu  
67 et al., 2022). However, the performance of regression-based methods is frequently  
68 constrained by the inherent nonlinearity in the relationships between model parameters  
69 and catchment descriptors, coupled with the difficulty in adequately capturing spatial  
70 heterogeneity, especially within complex mountainous terrain (Wu et al., 2022).

71 Recent advances in machine learning offer potential solutions by capturing  
72 nonlinear patterns in high-dimensional data. Such as Decision Tree (DT), Extremely  
73 Randomized Trees (ERT), Gradient Boosting Machine (GBM), K-Nearest Neighbor  
74 (KNN), Random Forest (RF), and Support Vector Machines (SVM) have shown  
75 promise in parameter regionalization (Golian et al., 2021; Song et al., 2022). However,  
76 existing machine learning-based parameter regionalization studies predominantly focus  
77 on runoff prediction at coarser temporal scales (daily or monthly) (Li et al., 2022; Wu  
78 et al., 2022), leaving a significant gap in high-resolution (hourly or sub-hourly) flood  
79 prediction in ungauged mountainous catchments. Moreover, these studies often rely on  
80 single machine learning methods to estimate all hydrological model parameters (Golian  
81 et al., 2021; Song et al., 2022; Wu et al., 2022). Given that different machine learning  
82 methods operate on distinct principles (Jordan et al., 2015; Zounemat-Kermani et al.,  
83 2021) and hydrological model parameters represent diverse hydrological processes (Li



84 et al., 2024), a single machine learning method may not adequately capture the  
85 complexity of model parameter estimation (Golian et al., 2021; Wu et al., 2022).  
86 Therefore, exploring the multi-machine learning ensemble methods is essential to  
87 improve the accuracy of high-resolution flood prediction in ungauged mountainous  
88 catchments.

89 Southwest China's mountainous regions are particularly vulnerable to frequent  
90 floods, leading to ecosystem degradation through habitat disruption and biodiversity  
91 loss (Gan et al., 2018). The abundance of ungauged catchments in this region poses a  
92 significant challenge to reliable flood prediction. To address this critical issue, we  
93 systematically evaluate the performance of a novel multi-machine learning ensemble  
94 method for regionalizing Top-SSF model parameters across 80 representative  
95 catchments (mean area: 1,586 km<sup>2</sup>) in Southwest China. By assessing ensemble method  
96 robustness under climate change and with varying donor catchment configurations, this  
97 study aims to significantly enhance flood prediction accuracy in ungauged mountainous  
98 catchments, contributing to improved ecosystem resilience, enhanced human safety,  
99 and more effective water resource management in the face of escalating climatic  
100 pressures.

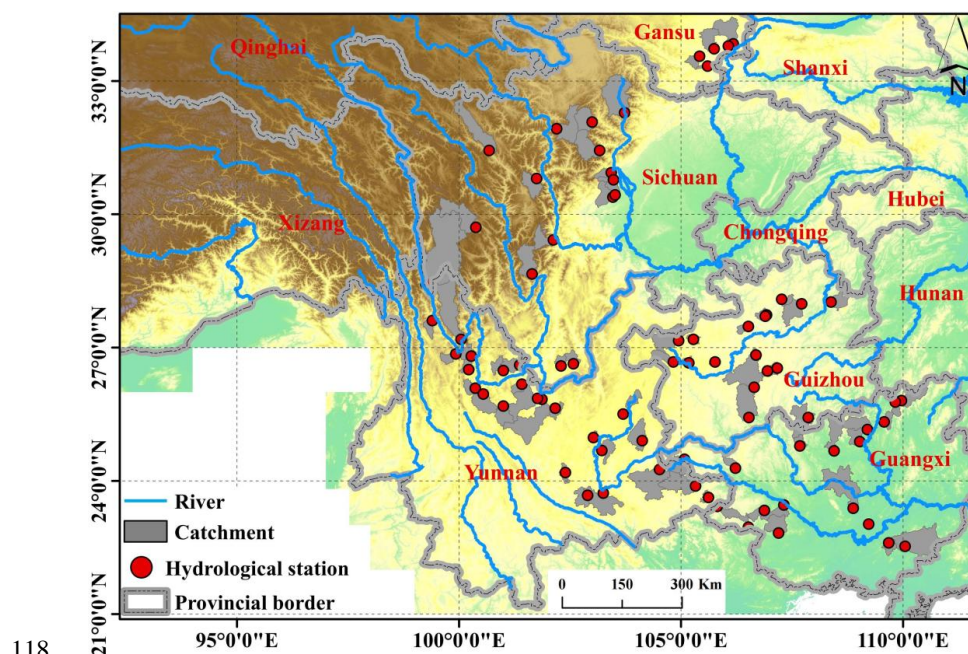
## 101 **2. Study area and datasets**

### 102 **2.1. Study area**

103 This study investigated 80 mountainous catchments in Southwestern China,  
104 encompassing Sichuan, Yunnan, Guangxi, Guizhou, and Chongqing provinces (Fig. 1).  
105 This region exhibits diverse climatic zones, including subtropical monsoon, plateau



106 mountain, and tropical monsoon climates. The selected catchments have an average  
107 area of 1,586 km<sup>2</sup>, with elevations ranging from 63 to 6,284 meters. Mean annual  
108 temperature varies from 15 to 20°C, and annual precipitation ranges from 1,200 to  
109 1,800 mm (Li et al., 2016), with approximately 80% of the annual precipitation  
110 occurring during summer and autumn, contributing to frequent flooding events (Cheng  
111 et al., 2019). These catchments are situated within a heavily forested region, the second  
112 largest in China (Hua et al., 2018), with forest cover ranging from 3% to 92% (mean:  
113 51%), influencing evapotranspiration and runoff generation. Dominant soil types  
114 include purple soil (12.20%), yellow soil (11.39%), and red soil (9.52%), each with  
115 distinct hydrological properties. Soil data were obtained from the Resource and  
116 Environmental Science and Data Center of the Chinese Academy of Sciences  
117 (<https://www.resdc.cn>).





119 **Fig.1.** Geographical distribution of the 80 gauged catchments used, with locations of  
120 hydrological stations (red points) and major rivers indicated.

## 121 **2.2. Datasets**

122 Hourly flood data (2015–2018) for 80 mountainous catchments in China were  
123 sourced from the Hydrological Bureau of the Ministry of Water Resources, through  
124 China's hydrologic yearbooks. Hourly rainfall data (2015–2018) were obtained from  
125 ground meteorological stations across China (<http://en.weather.com.cn>), providing  
126 crucial input for hydrological modelling. Additional meteorological variables,  
127 including temperature, wind speed, dewpoint temperature, and surface net solar  
128 radiation, were obtained from the ERA5 hourly dataset (1940–present) (Hersbach et al.,  
129 2023), ensuring comprehensive atmospheric forcing. Relative humidity was estimated  
130 using dewpoint temperature. Historical (1901–2021) and projected future (SSP585,  
131 2022–2100) temperature and precipitation data for China, averaged from the EC-Earth3,  
132 GFDL-ESM4, and MRI-ESM2-0 models at 1 km resolution, were obtained from "A  
133 Big Earth Data Platform for Three Poles" to assess the impact of climate change (Ding  
134 et al., 2020) (<http://poles.tpc.ac.cn>). Topographic data, including a 30-m resolution  
135 Digital Elevation Model (DEM), used for river network and topographic index  
136 derivation, were obtained from EARTHDATA and used for river network delineation  
137 and topographic index derivation (<https://search.earthdata.nasa.gov/search>). Forest  
138 cover data (30-m resolution) were sourced from the Global Forest Cover and Forest  
139 Change Map (<https://www.noda.ac.cn/>), providing information on vegetation  
140 characteristics. Bulk density (BD) data were derived from the Soil Database of China  
141 for Land Surface Modelling (Dai et al., 2013). Soil hydraulic parameters, specifically



142 saturated hydraulic conductivity (Ks\_CH) for Clapp and Hornberger functions and the  
143 pore-connectivity parameter (L) for van Genuchten and Mualem functions, were  
144 acquired from the China Dataset of Soil Hydraulic Parameters Using Pedotransfer  
145 Functions for Land Surface Modeling (Shangguan et al., 2013).

146 **Table 1.** Model forcing data and catchment descriptors information.

Data type	Name	Unit	Function
Hydro-meteorology	Rainfall	mm	Input for hydrological model
	Flood	m <sup>3</sup> /s	Used for model calibration (hourly resolution)
	Temperature	K	Input for hydrological model
	Surface pressure	Pa	
	Dewpoint temperature	K	
	wind speed	m/s	
	Surface net solar radiation	j/m <sup>2</sup>	
	Relative humidity	%	Multi-year surface average as catchment descriptors
	1 km monthly precipitation (1901-2021)	mm	
	1 km monthly temperature (1901-2021)	°C	
	1 km monthly temperature (2022-2100, SSP5-8.5, EC-Earth3, GFDL-ESM4, MRI-ESM2-0)	°C	
	1 km monthly precipitation (2022-2100, SSP5-8.5, EC-Earth3, GFDL-ESM4, MRI-ESM2-0)	mm	
Soil characteristics	Soil bulk density (BD)	g/cm <sup>3</sup>	Surface average as catchment descriptors
	Pore-connectivity parameter (L) for the van Genuchten and Mualem functions	-	
	Saturated hydraulic conductivity (Ks_CH) of the Clapp and Hornberger Functions	cm d <sup>-1</sup>	
Topography	Forest cover (FC)	%	Surface average as catchment descriptors
	DEM	m	
	Topographic index	-	
	Slope	mm <sup>-1</sup>	
	Catchment area	km <sup>2</sup>	

### 147 3. Methodology

#### 148 3.1. Hydrological model

149 The Top-SSF model, inheriting the straightforward structure, physical  
150 interpretability, and ease of parameter transferability from the original TOPMODE  
151 (Beven et al., 2021; Gao et al., 2018), consists of 15 parameters representing six key  
152 hydrological components: canopy interception, infiltration, evapotranspiration,  
153 unsaturated zone moisture transport, subsurface storm flow, and flow routing (Li et al.,





2024). In the Top-SSF model, flood can be comprised of four components: infiltration-excess overland flow, saturation-excess overland flow, subsurface storm flow, and groundwater discharge.

Infiltration-excess overland flow occurs when the rainfall intensity exceeds the infiltration capacity. In this study, infiltration is simulated using the Green-Ampt model. When surface ponding occurs, the infiltration rate is determined by solving the Green-Ampt equation iteratively, for which the Newton-Raphson method is employed. The infiltration rate ( $f_{in}$ ) is given by:

$$f_{in} = -\frac{Ks(CD+F_{satrt})}{Szm(1-e^{(F_{satrt}/Szm)})} \quad (1)$$

where,  $f_{in}$  is the infiltration rate (m/h);  $Ks$  is surface hydraulic conductivity (m/h);  $CD$  is capillary drive (m);  $F_{satrt}$  is the initial cumulative infiltration (m);  $Szm$  is the maximum water storage capacity in the unsaturated zone (m).

Saturation excess overland flow occurs at computational cell  $i$  when the groundwater table depth,  $S_i$  is less than or equal to zero (i.e.,  $S_i \leq 0$ , indicating the water table has reached the surface). It is calculated as:

$$r_{s,i} = \max\{Suz_i - \max(S_i, 0), 0\} \quad (2)$$

where,  $r_{s,i}$  is the depth of saturation excess overland flow generated at cell  $i$  (m);  $Suz_i$  is the soil water storage in the unsaturated zone, at cell  $i$  (m);  $S_i$  is the groundwater table depth at cell  $i$  (m).

The depth of storm subsurface flow generated at computational cell  $i$ ,  $r_{sf,i}$  is given by:

$$r_{sf,i} = q_{sf0}(1 - S_{sf,i}/S_{fmax}) \quad (3)$$

where,  $r_{sf,i}$  is the depth of storm subsurface flow at cell  $i$  (m);  $q_{sf0}$  is initial subsurface storm flow (m);  $S_{sf,i}$  is the water storage deficit in the storm subsurface flow zone at cell  $i$  (m).

The depth of groundwater discharge is calculated as:



180 
$$r_b = e^{\ln Te - \lambda - \bar{S}_g / Sz m} \quad (4)$$

181 where,  $r_b$  is depth of groundwater discharge (m);  $\ln Te$  is the log of the areal average of  
182  $T0$  ( $m^2/h$ ); is the catchment average topographic index;  $\bar{S}_g$  is the catchment average  
183 groundwater table depth (m). For the complete set of equations for the Top-SSF model,  
184 the reader is referred to the Supplementary Material and (Li et al., 2024).

185

### 186 **3.2. Multi-machine learning ensemble method**

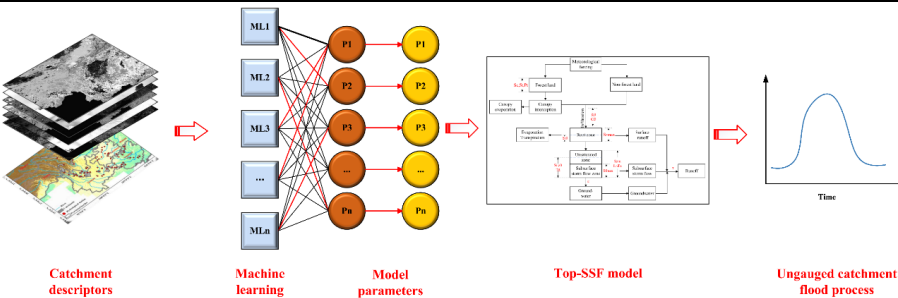
187 To improve flood prediction accuracy in ungauged mountainous catchments, we  
188 proposed a multi-machine learning ensemble method for regionalizing sensitive  
189 parameters of the Top-SSF model. This method leverages the complementary strengths  
190 of multi-machine learning methods to estimate model parameters based on catchment  
191 descriptors (Fig. 2). The characteristics, strengths, and limitations of each machine  
192 learning method are summarized in Table 2. The ensemble method employs a cross-  
193 validation procedure to select the best-performing machine learning method for each  
194 sensitive parameter. These selections are then integrated into a unified regionalization  
195 scheme. By mitigating limitations inherent in single machine learning regionalization,  
196 such as model bias and overfitting, and by capturing complex hydrological processes  
197 in mountainous catchment, this ensemble method aims to achieve more accurate flood  
198 prediction in ungauged catchments.

199



200 **Table.2.** Seven machine learning model characteristics, advantages and disadvantages.

Machine learning	Characteristic	Advantage	Disadvantages
DT	A single decision tree hierarchically partitions the data space using a tree structure, with internal nodes representing features, branches representing decision rules, and leaf nodes representing class labels.	High interpretability; Minimal data preprocessing.	Unstable; Tends to overfit.
ERT	Construct multiple decision trees with randomly selected feature values and randomly divided nodes (Geurts et al., 2006).	Low overfitting risk; Computational efficiency; Resilient to noise.	Possibility of increased bias; Limited interpretability.
GBM	Construct multiple decision trees. Multiple weak learners are trained iteratively and the loss function is optimised using gradient descent, progressively combined into a robust model through the learning rate (Friedman, 2002).	High accuracy for structured data; Robust to outliers; Minimal data preprocessing.	Limited interpretability; Complex adjustments.
KNN	It is a non-parametric, instance-based supervised learning algorithm. It operates by finding the K nearest data points in the training data to a given data point and making predictions based on these (Wani et al., 2017).	Simple and easy to implement. Learning process is quick.	Sensitivity to noisy and scale of data. Accuracy can be heavily impacted by the choice of K.
RF	A bagging algorithm proposed by Breiman (2001) that uses ensemble learning. Involves training numerous decision trees and aggregating predictions.	Simple and easy to implement; Low computational cost.	Prone to overfitting in noisy regression tasks.
SVM	Identifies hyperplanes in high-dimensional spaces to segregate data. The optimal hyperplane maximizes the margin between it and the nearest data points, termed support vectors (Sain, 1996).	Uses kernel functions to address nonlinear classification issues.	Sensitive to noise



201 **Fig.2.** Multi-machine learning ensemble method for regionalization in ungauged mountainous  
202 catchments. The red line indicates the machine learning method that yielded the optimal  
203 parameter estimates.  
204

205 **3.3. Parameter regionalization process**

206 The parameter regionalization process comprised four key steps: (1) Top-SSF  
207 model calibration and parameter sensitivity analysis; (2) selection of relevant catchment  
208 descriptors; (3) establishment of regionalization relationships between sensitive model  
209 parameters and catchment descriptors using multi-machine learning ensemble methods;



210 and (4) evaluation of parameter regionalization performance.

### 211 **3.3.1. Top-SSF model calibration and parameter sensitivity analysis**

212 The model was calibrated and validated using two and one flood events each  
213 catchment, respectively. The Nash-Sutcliffe Efficiency (NSE) served as the objective  
214 function during calibration, with parameter optimization achieved using the Shuffled  
215 Complex Evolution (SCE-UA) algorithm (Duan et al., 1994), known for its global  
216 convergence and robustness (Dakhlaoui et al., 2012; Qi et al., 2016). Model  
217 performance was evaluated using the NSE,  $Q_p$ , and  $T_p$ , following China's Specification  
218 for Hydrological Information Forecast (GB/T 22482-2008). These metrics quantify the  
219 model's ability to predict flood dynamics, peak flow, and timing. Following calibration,  
220 a sensitivity analysis was conducted to identify and exclude insensitive model  
221 parameters (Lenhart et al., 2002), which were then used for regionalization. This  
222 approach reduces the dimensionality of the regionalization problem and improves the  
223 efficiency of the process.

224 The sensitivity index ( $Si$ ) of each hydrological model parameter was determined  
225 using the method of Lenhart et al. (2002), which assesses the influence of  $\pm 10\%$   
226 changes in parameter values (Eq. 1). Table 2 outlines the sensitivity analysis results for  
227 the model parameters across the 80 mountainous catchments. The  $Si$  values are  
228 categorized as follows (Guo et al., 2022): negligible sensitivity ( $|Si| < 0.05$ ),  
229 moderate sensitivity ( $0.05 < |Si| < 0.2$ ), high sensitivity ( $0.2 < |Si| < 1.00$ ), and  
230 extremely high sensitivity ( $|Si| \geq 1.00$ ). Based on the sensitivity analyses, seven  
231 sensitive model parameters were identified:  $Szm$ ,  $lnTe$ ,  $Sfmax$ ,  $C$ ,  $qsfo$ ,  $t$  (Table 2).



$$Si = \frac{1}{N} \sum_t^N \frac{(y_2(t) - y_1(t)) / y_0(t)}{2\Delta x / x_0} \quad (5)$$

where  $y_0(t)$  is the flood value of the calibrated parameter  $x_0$  at time  $t$ ;  $\Delta x$  is the adjusted parameter difference,  $\Delta x / x_0 = 10\%$ ;  $y_1(t)$  is the flood value of the calibrated parameter  $x_0 - \Delta x$  at time  $t$ ;  $y_2(t)$  is the flood value of the calibrated parameter  $x_0 + \Delta x$  at time  $t$ .

**Table 2.** Top-SSF model main modules and default range of parameters.

Modular	Parameter	Definition	Unite	Default range	Sensitivity index
Canopy interception	$Sc$	Canopy storage capacity	m	0.00~0.01	<0.05
	$St$	Trunk storage capacity	m	0.00~0.01	<0.05
	$Pt$	Proportion of rain diverted into stemflow per cove	%	0.00~1.00	<0.05
Evapotranspiration	$Sr0$	Initial root zone storage deficit	m	0.00~0.02	<0.05
	$Srmax$	Maximum root zone storage deficit	m	0.00~2	<0.05
Infiltration	$Ks$	Surface hydraulic conductivity	m/h	0~0.01	<0.05
	$CD$	Capillary drive (Morel-Seytoux et al., 1974)	m	0~5	<0.05
Unsaturated zone	$Suz0$	Initial baseflow per unit area	m	0.00~ $10^{-4}$	<0.05
	$Szm$	Soil maximum water storage capacity	m	0.00~1.00	<b>0.19</b>
	$td$	Unsaturated zone time delay per unit storage deficit	h/m	0~3	<b>1.07</b>
	$lnTe$	log of the areal average of T0	m <sup>2</sup> /h	-2.00~1.00	<b>3.4</b>
Subsurface storm flow zone	$Sfmax$	Maximum subsurface storm flow zone deficit	m	0.00~0.01	<b>0.16</b>
	$C$	Transfer coefficient	m <sup>-2</sup> /h	0.00~0.1	<b>0.26</b>
	$qsfo$	Initial subsurface storm flow per unit area	m	0.00~0.02	<b>0.18</b>
Routing	$t$	Flow routing correction coefficient	-	0.00~5.0	<b>1.21</b>

**Note, the bolded values in the sensitivity index indicate sensitive model parameters.**

### 3.3.2. Catchment descriptor selection

To mitigate the effects of multicollinearity on the accuracy and reliability of the parameter regionalization methods, catchment descriptors were screened using the variance inflation factor (VIF) and correlation coefficients. A VIF threshold of less than 10 (VIF < 10) was used to indicate acceptably low multicollinearity (Salmeron et al.,



2018). Initial analysis revealed strong correlations between specific catchment descriptors, namely L and Ks\_CH, and Tem and Elev, indicating potential redundancy. Furthermore, the VIF for Ks\_CH and Slope exceeded 10, suggesting substantial multicollinearity, should be removed. Despite this, Tem was retained as a descriptor due to its importance in representing climate change impacts. Fig. 3b illustrates the correlation coefficients between eight catchment descriptors (including Tem) and the sensitive model parameters. These correlations, with the highest reaching only 0.5 (e.g., between *qsfo* and Pre), suggest that the relationships between the catchment descriptors and sensitive model parameters are complex and nonlinear. The final set of catchment descriptors used for parameter regionalization comprised FC, Elev, Area, L, Tem, Prec, and BD.

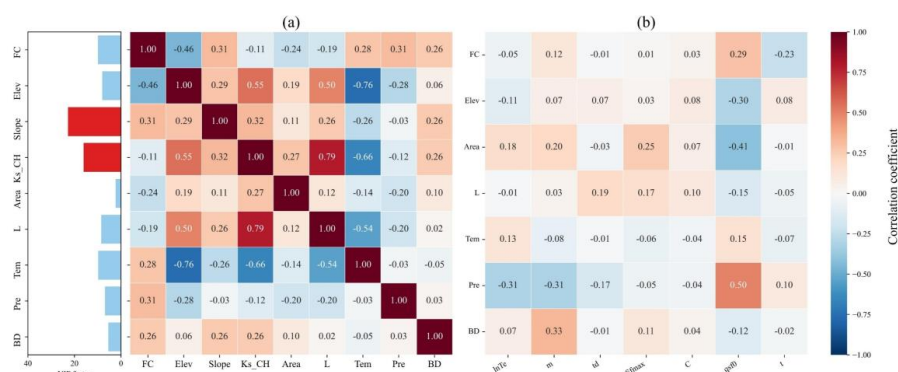


**Fig.3.** Analysis of catchment descriptor relationships: (a) Correlation coefficients and variance inflation factors (VIF) among all descriptors; (b) Correlation coefficients between sensitivity model parameters and descriptors with VIF values below 10.

### 3.3.3. Parameter regionalization

To simulate ungauged catchment conditions, each of the 80 catchments was iteratively treated as an ungauged catchment, with the remaining 79 catchments serving as donor catchments. A parameter regionalization method was then constructed using



the catchment descriptors and sensitive model parameters of the donor catchments to predict the seven sensitive model parameters for the ungauged catchment based on its catchment descriptors. These predicted model parameters were then input into the Top-SSF model to enable flood prediction in ungauged catchments. To ensure robust and generalizable results, K-fold cross-validation ( $K = 10$ ) was implemented. This involved randomly partitioning the 79 donor catchments into K subsets, using one subset as a test set and the remaining K-1 subsets for method training in each iteration (Jung, 2018). This approach maximizes data utilization and minimizes bias associated with specific data partitioning. Hyperparameter tuning for each machine learning method was performed using RandomizedSearchCV (Bergstra et al., 2012), with the objective of minimizing the difference between predicted and observed parameter values.

#### 3.3.4. Evaluated metrics

The performance of the parameter regionalization methods was evaluated by considering two key aspects. First, the accuracy of the methods in estimating sensitive model parameters was assessed using three metrics: root mean square error (RMSE), standard deviation (STD), and the coefficient of determination ( $R^2$ ). The  $R^2$  was used to quantify the agreement between estimated and calibrated parameter sets. Second, to evaluate the impact of parameter regionalization on flood prediction. The resulting flood predictions were then evaluated using the NSE, Qp, and Tp metrics.

$$NSE = 1 - \frac{\sum_{j=1}^M (Q_{obs}(j) - Q_{sim}(j))^2}{\sum_{j=1}^M (Q_{obs}(j) - \bar{Q}_{obs})^2} \quad (6)$$

$$Q_p = \left| \frac{Q_{obs,p} - Q_{sim,p}}{Q_{obs,p}} \times 100\% \right| \quad (7)$$

$$T_p = |T_{obs,p} - T_{sim,p}| \quad (8)$$



285 where  $Q_{obs}(j)$  is the observed flow rate ( $\text{m}^3/\text{s}$ );  $Q_{sim}(j)$  is the simulated flow rate  
286 ( $\text{m}^3/\text{s}$ );  $\bar{Q}_{obs}$  is the mean value of the observed flow rate ( $\text{m}^3/\text{s}$ );  $Q_{obs,p}$  is the observed  
287 flood peak flow ( $\text{m}^3/\text{s}$ );  $Q_{sim,p}$  is the simulated flood peak flow ( $\text{m}^3/\text{s}$ );  $T_{obs,p}$  is the  
288 observed flood peak occurrence time (h); and  $T_{sim,p}$  is the simulated flood peak  
289 occurrence time (h).

290

$$291 \quad RMSE = \sqrt{\frac{1}{N} \sum_{i=1}^N (X_i - Y_i)^2} \quad (9)$$

$$292 \quad STD = \sqrt{\frac{1}{N-1} \sum_{i=1}^N (Y_i - \bar{Y})^2} \quad (10)$$

$$293 \quad R^2 = \frac{[\sum_{i=1}^N (X_i - \bar{X})(Y_i - \bar{Y})]^2}{\sum_{i=1}^N (X_i - \bar{X})^2 \sum_{i=1}^N (Y_i - \bar{Y})^2} \quad (11)$$

294 where  $X_i$  is the Top-SSF calibration model parameter value;  $Y_i$  is the model parameter  
295 estimated value using the parameter regionalization method;  $\bar{X}$  and  $\bar{Y}$  are the mean  
296 values of  $X_i$  and  $Y_i$ ;  $N$  is the sample size equal to 80.  
297



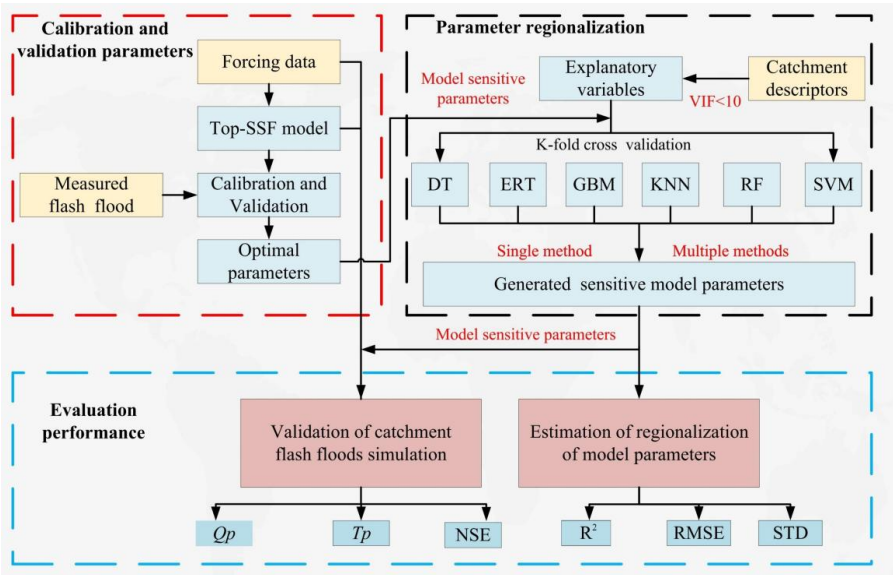


**Fig.4.** Flowchart illustrating the parameter calibration, validation, and regionalization workflow. Abbreviations: Top-SSF (Topography-Based Subsurface Storm Flow hydrological model), DT (Decision Tree), ERT (Extremely Randomized Trees), GBM (Gradient Boosting Machine), KNN (K-Nearest Neighbor), RF (Random Forest), SVM (Support Vector Machine), NSE (Nash-Sutcliffe efficiency),  $R^2$  (Coefficient of Determination),  $Q_p$  (Relative error of flood peak flow),  $T_p$  (Relative error of flood peak occurrence time), VIF (Variance inflation factor), RMSE (Root mean square error), STD (Standard deviation).

## 4. Result

### 4.1. Model performance

The Top-SSF model demonstrated good flood simulation performance across the 80 gauged catchments, as quantified by NSE,  $Q_p$ , and  $T_p$ . During the calibration period, 50% of the catchments achieved NSE values exceeding 0.78 (Fig. 5a), the median  $Q_p$  value was below 10% (Fig. 5b), and the median  $T_p$  value was within 2 hours (Fig. 5c). The average NSE value was approximately 0.8, with a maximum of 0.96. The majority of  $Q_p$  values were around 8%, and the majority of  $T_p$  values were below 2 hours. During the validation period, the median NSE value was 0.76 (Fig. 5a), the median  $Q_p$



value was below 10% (Fig. 5b), and the median  $T_p$  value was within 4 hours (Fig.5c). Model performance also exhibited some dependence on catchment characteristics. For instance, NSE generally improved with increasing forest cover (Fig. 6a), potentially due to the model's explicit representation of forest canopy interception and subsurface storm flow generation mechanisms. The relationship between NSE,  $Q_p$ ,  $T_p$  and elevation was more complex, suggesting a nonlinear influence of elevation on model performance (Fig. 6a-c). The demonstrated robust performance of the Top-SSF model provides a strong foundation for its application in subsequent parameter regionalization analyses.

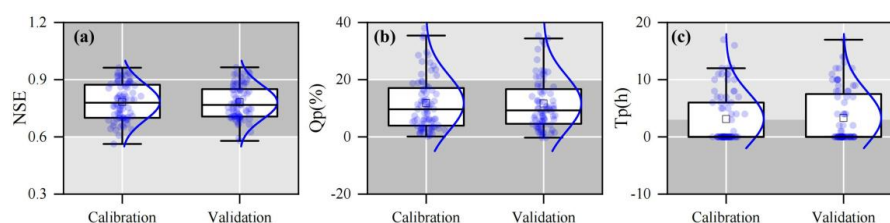


**Fig. 5.** Boxplots of (a) NSE, (b)  $Q_p$ , and (c)  $T_p$  during the calibration and validation periods for 80 gauged catchments. The box represents the interquartile range, with the middle line indicating the median (50th percentile). The whiskers represent the minimum and maximum values. "□" represents the mean value. Dark grey indicates the range of flood prediction criteria (i.e.,  $NSE > 0.75$ ,  $Q_p < 20\%$ , and  $T_p < 2$  hours).

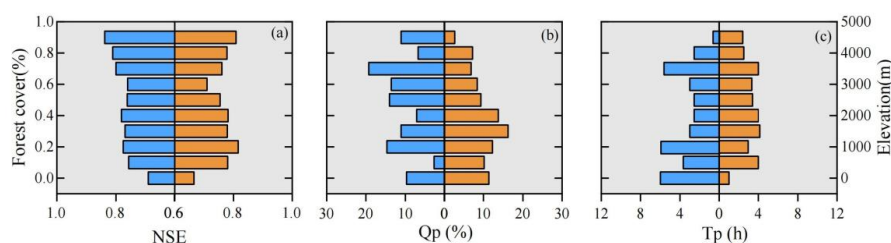


**Fig.6.** Influence of environmental factors on Top-SSF model performance in flood simulation. The graphs illustrate the relationship between model evaluation metrics and forest cover (left) and elevation (right)."



## 336 **4.2. Results of parameter regionalization**

### 337 **4.2.1. Comparison of sensitive model parameter estimates**

338 The six single machine learning parameters regionalization methods exhibited  
339 varying performance in estimating sensitive model parameters (Fig. 7), likely due to  
340 differences in catchment descriptor characteristics and the underlying principles of each  
341 method. GBM demonstrated the highest accuracy in estimating  $Szm$ ,  $td$ , and  $C$  ( $R^2 =$   
342  $0.90, 0.86$ , and  $0.87$ , respectively), with its estimates also exhibiting a STD that closely  
343 matched the distribution of the calibrated parameter values. KNN provided the most  
344 accurate estimates for  $lnTe$ ,  $qsfo$ , and  $t$  ( $R^2 = 0.87, 0.89$ , and  $0.90$ , respectively), also  
345 with STD closely resembling the calibrated parameter distributions. RT performed best  
346 in estimating  $Sfmax$  ( $R^2 = 0.87$ ), but its performance was generally poorer for other  
347 parameters. DT, SVM, and RF methods generally showed lower performance across all  
348 sensitive model parameters. These differences in performance highlight the potential  
349 benefits of multi-machine learning ensemble methods for improving flood prediction  
350 in ungauged mountainous catchments.

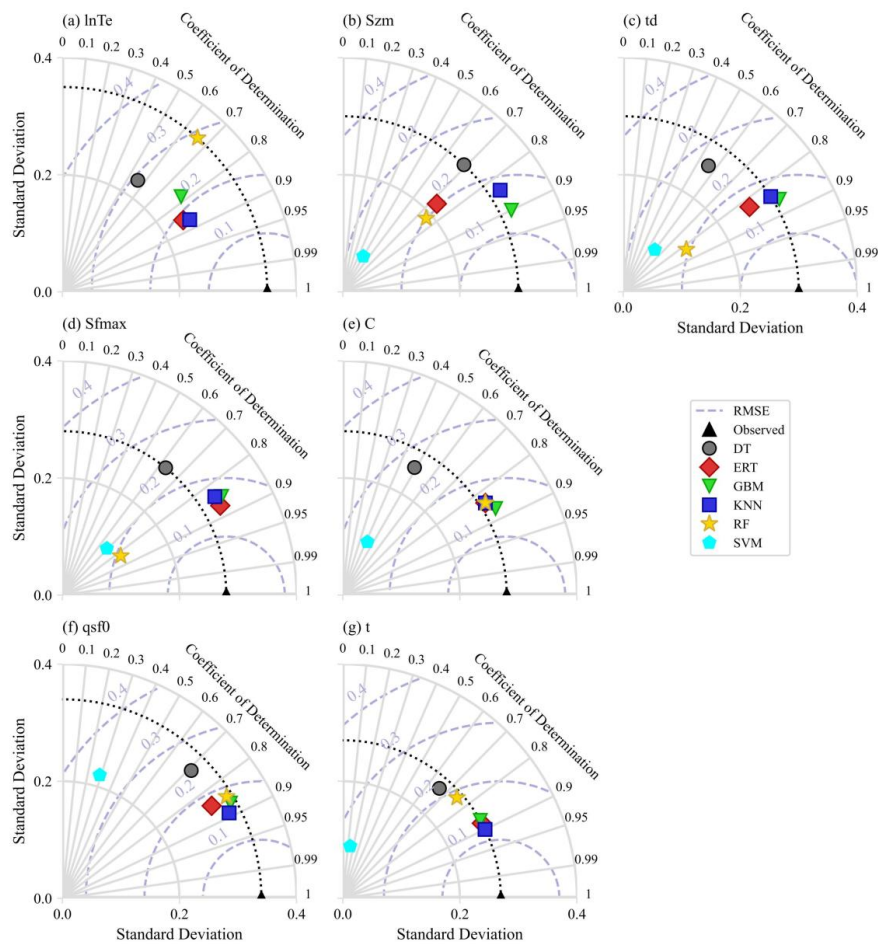


**Fig.7.** Performance of parameter regionalization methods assessed using Taylor diagrams. The diagrams show the accuracy of sensitive model parameter estimates, with the coefficient of determination ( $R^2$ ) indicated by the radial axis, standard deviation (STD) by the horizontal and vertical axes, root mean square error (RMSE) by the grey-blue dotted lines, and the standard deviation of observations by the black dotted line."

#### 4.2.2. Comparison of flood forecasting results

The flood prediction performance of the Top-SSF model, integrated with different parameter regionalization methods, was compared across 80 mountainous catchments in southwestern China. The methods included single machine learning methods and a multi-machine learning ensemble method (GBM-KNN-ERT), where GBM estimated



362  $Szm$ ,  $td$ , and  $C$ ; KNN estimated  $lnTe$ ,  $qsfo$ , and  $t$ ; and ERT estimated  $Sfmax$ . The  
363 performance of these parameter regionalization methods was then evaluated against the  
364 performance of the Top-SSF model using calibrated parameter. Among the single  
365 machine learning methods, GBM performed best. Approximately 75% of the  
366 catchments achieved NSE greater than 0.9 (Fig. 8a), Qp less than 5% (Fig. 8b), and Tp  
367 less than 1 hour (Fig. 8c). These results surpass the flood prediction standards outlined  
368 in the Specification for Hydrological Information Forecast of China (GB/T 22482-2008;  
369  $NSE > 0.75$ ,  $Qp < 20\%$ ,  $Tp < 2$  hours). The GBM-KNN-ERT method yielded even  
370 better results than the GBM. With GBM-KNN-ERT, 75 of the catchments had  $NSE >$   
371 0, and 90% of the catchments had  $NSE > 0.9$ . The Qp values were also more  
372 concentrated near 0, and while the Tp values exhibited a slightly broader distribution,  
373 90% of the catchments still had Tp values near 0. These results strongly suggest the  
374 potential of multi-machine learning ensembles for improving flood prediction in  
375 ungauged catchments.

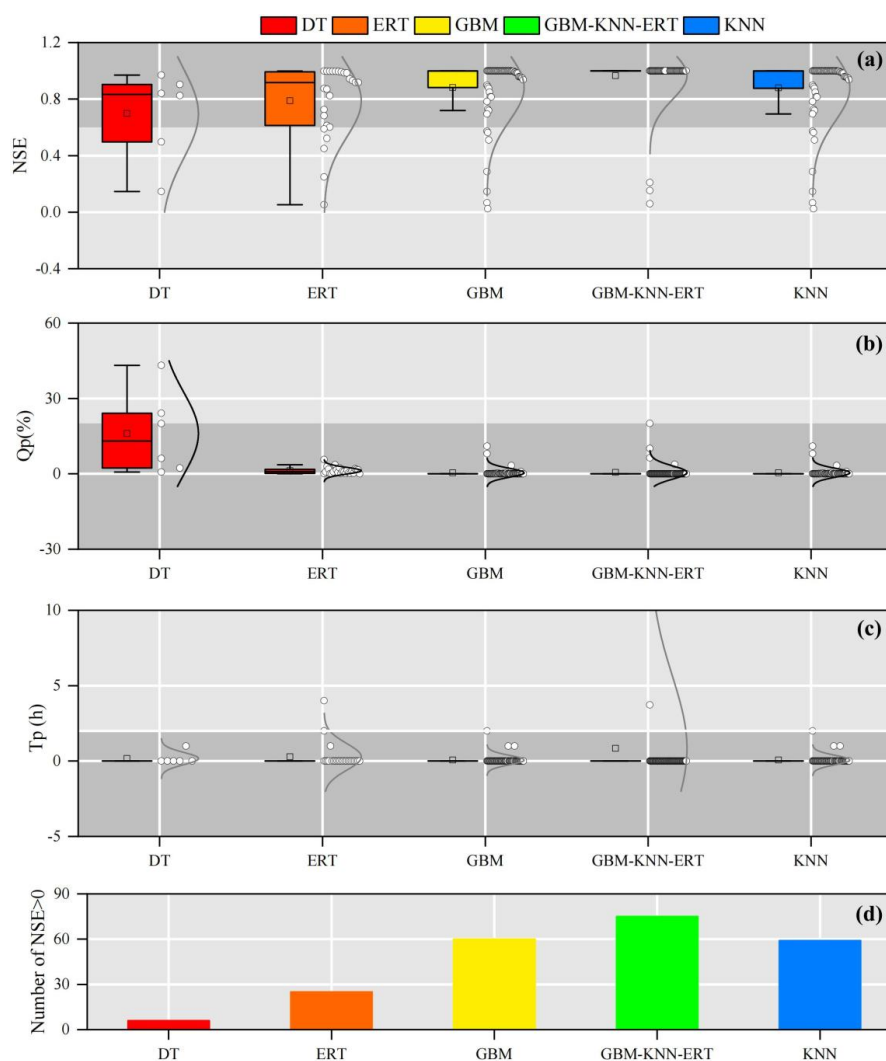


**Fig.8.** Evaluation of flood prediction performance achieved by different parameter regionalization methods, relative to the calibrated Top-SSF model. Boxplots and normal distribution curves illustrate the distribution of (a) NSE, (b) Qp, (c) Tp, and (d) the number of catchments exceeding NSE > 0. Shaded regions highlight where flood prediction standards were met (NSE > 0.75, Qp < 20%, Tp < 2 hours).



## 382 5. Discussion

### 383 5.1. Reliability of multi-machine learning ensemble in parameter regionalization

384 In this study, the GBM-KNN-ERT method demonstrated superior parameter  
385 regionalization performance in ungauged mountainous catchments, highlighting the  
386 potential of multi-machine learning methods for improving hydrological predictions in  
387 ungauged mountainous catchments. The GBM method exhibited distinct parameter-  
388 specific sensitivities to hyperparameters (Fig. 9a-c). For parameter  $C$ , the negative  
389 correlation between  $R^2$  and  $n\_estimators$  ( $>500$  trees) indicates overfitting risks when  
390 modeling complex rainfall-runoff interactions in heterogeneous mountainous terrain  
391 (Fig. 9a). This aligns with previous findings emphasizing the need for complexity  
392 control in hydrological generalization (Schoups et al., 2008). Conversely, the improved  
393  $R^2$  for parameter  $td$  with increased  $n\_estimators$  highlights the capacity of ensemble  
394 learning to capture complex, nonlinear relationships between catchment descriptors and  
395 hydrological parameters (Hastie et al., 2009). The contrasting optimal  $max\_depth$  of 5  
396 layers for parameter  $C$ , compared to shallower optimal depths (3 layers) for  $Szm$  and  
397  $td$ , suggests that parameters governing more complex hydrological processes in  
398 mountainous catchments may require deeper decision trees to effectively capture the  
399 interactions between climate, topography, and soil properties (Wainwright et al., 2013).

400 KNN performance exhibited pronounced sensitivity to neighborhood size  
401 ( $n\_neighbors$ ) and distance metric ( $p$ ), highlighting the spatial heterogeneity of  
402 catchment descriptors. For parameters  $lnTe$  and  $qsfo$ , optimal performance was  
403 observed at  $n\_neighbors=20$  (Fig. 9d). This aligns with the hypothesis that meaningful



404 hydrological similarities can emerge even in topographically complex mountainous  
405 regions when considered at broader spatial scales (Li et al., 2022). Conversely,  
406 parameter  $t$  achieved peak accuracy at  $n\_neighbors=5$ , suggesting that localized, short-  
407 term weather events and fine-scale topographic similarities in adjacent mountainous  
408 areas can significantly influence local runoff processes (Garambois et al., 2015). The  
409 Manhattan distance metric ( $p=1$ ) outperformed Euclidean distance across all  
410 parameters (Fig. 9e). This superiority stems from its ability to mitigate the "curse of  
411 dimensionality" (Bellman, 1961) in high-dimensional datasets, a common  
412 characteristic of mountainous catchments. In such datasets, sparse data distributions  
413 and the presence of mixed variable types (e.g., topographic indices, land cover) can  
414 significantly degrade the discriminative power of Euclidean distance (Rockström et al.,  
415 2023). The robustness of the Manhattan distance arises from its axis-aligned sensitivity,  
416 which provides a more effective means of handling feature scaling and integrating  
417 categorical descriptors compared to the radial symmetry of Euclidean distance.

418 ERT performance was maximized at  $max\_features = 0.15$  (Fig. 9f). By restricting  
419 the random sampling of features during node splits (using only 15% of the features),  
420 both the diversity of the trees was enhanced and the effects of multicollinearity between  
421 topographic and soil attributes were reduced. This finding aligns with the theory  
422 proposed by Geurts et al. (2006), which suggests that random feature selection can  
423 significantly improve model generalization, a particularly important consideration in  
424 ungauged mountainous catchments characterized by high levels of inter-correlation  
425 among predictor variables.



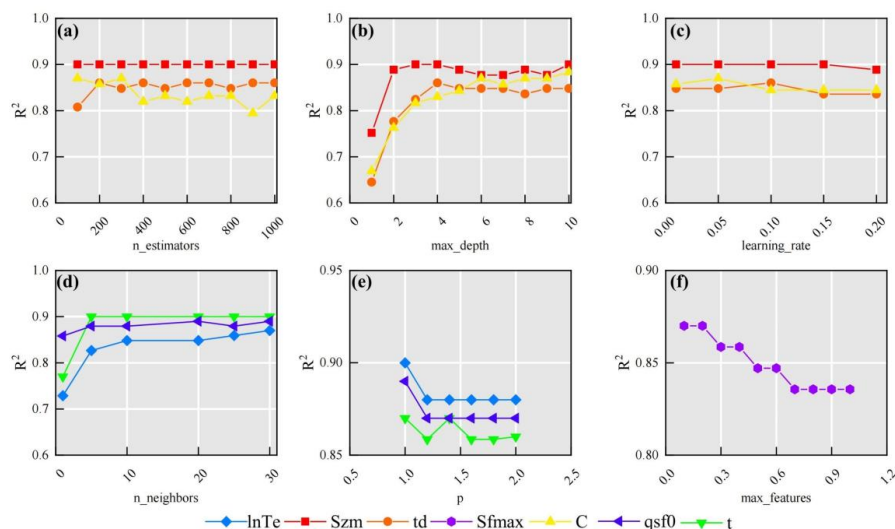


**Fig.9.** Sensitivity of parameter estimation performance to key hyperparameters in (a-c) GBM, (d-e) KNN method, and (f) ERT. (a) *n\_estimators* (number of decision trees in GBM), (b) *max\_depth* (maximum depth of decision trees in GBM), (c) *learning\_rate* (GBM), (d) *n\_neighbors* (number of neighbors in KNN), (e) *p*-value of Minkowski distance (KNN; *p*=1: Manhattan distance, *p*=2: Euclidean distance), and (f) *max\_features* (ERT).

## 5.2. Combining multiple machine learning methods for parameter regionalization

Machine learning methods exhibit distinct strengths in hydrological parameter estimation due to fundamental differences in data processing mechanisms, pattern recognition strategies, and prediction generation (Bishop et al., 2006). This suggests that multi-machine learning ensemble methods have the potential to synergistically integrate advantages while effectively compensating for individual limitations, leading to more robust and accurate parameter estimates. As demonstrated in Fig. 10, the GBM-KNN-ERT method achieved notable improvements over single machine learning method, particularly for sensitive parameters *lnTe*, *Sfmax*, *qsf0* and *t*, with  $R^2$  increases ranging from 0.02 to 0.03 compared to the best-performing GBM method (Fig.10e). Interestingly, a comparison of GBM4-KNN3 (where *Sfmax* is estimated by GBM) and GBM3-KNN4 (where *Sfmax* is estimated by KNN) revealed critical



444 insights into model parameter compatibility. Despite achieving identical  
445  $Sf_{max}$  estimation accuracy ( $R^2 = 0.85$ ), GBM4-KNN3 exhibited superior flood  
446 prediction performance, with 72 catchments achieving  $NSE > 0$  compared to only 68  
447 catchments for GBM3-KNN4. This suggests that GBM possesses an enhanced  
448 capability to resolve the complex coupling between soil moisture dynamics and  
449 topographic, leading to more accurate representation of subsurface storm flow  
450 processes (Gupta et al., 2023). The wider distribution of flood prediction performance  
451 observed for GBM3-KNN4 (Fig. 10a–c) further suggests that uncertainties introduced  
452 by KNN in the estimation of  $Sf_{max}$  may propagate nonlinearly during flood  
453 simulations, potentially amplifying errors. This observation aligns with theoretical  
454 expectations that distance-based methods may tend to over smooth critical thresholds  
455 or sharp transitions in heterogeneous environments, leading to a less accurate  
456 representation of hydrological responses (Bellman, 1961).

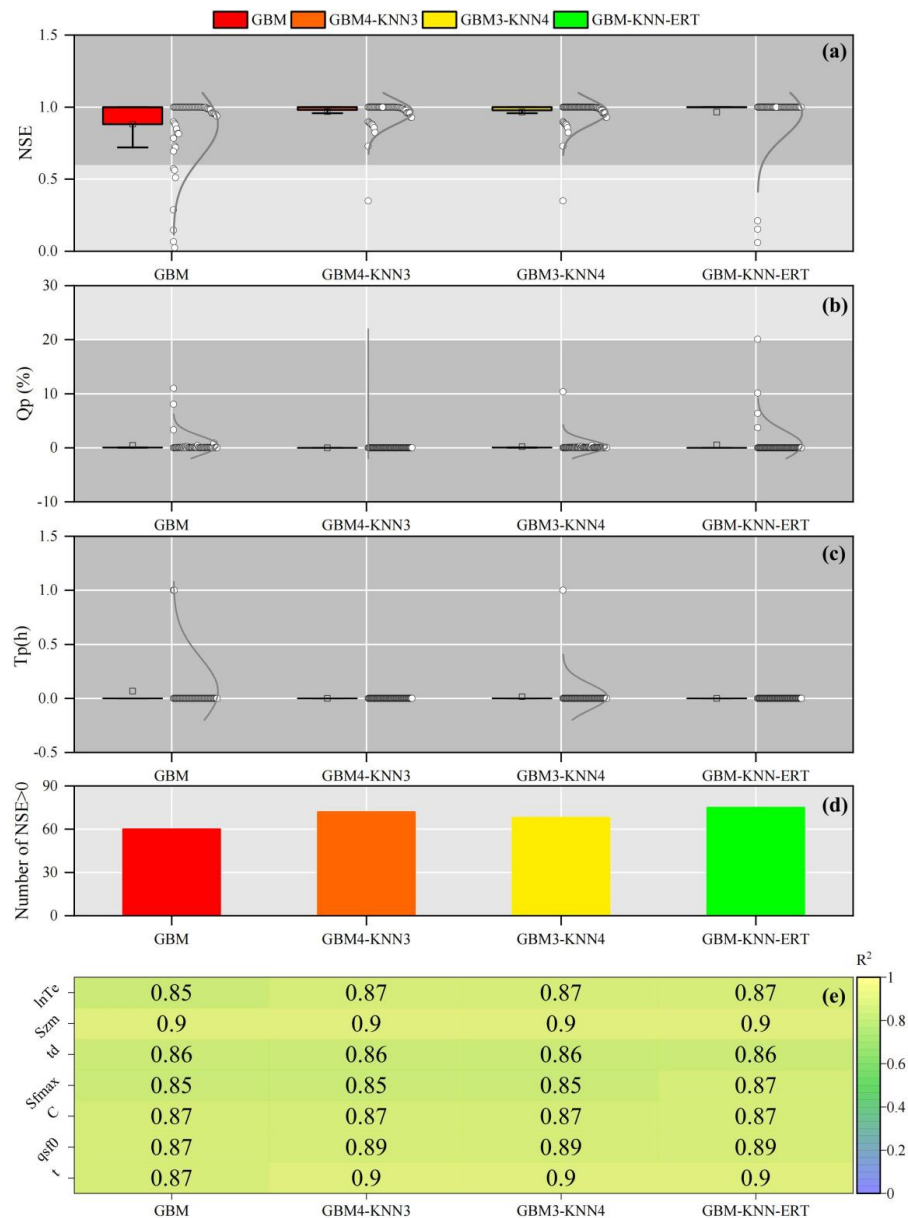


**Fig.10.** Assessment of combined machine learning methods for improved parameter regionalization in ungauged mountainous catchments. Performance is evaluated against the GBM method, showing (a) NSE, (b) Qp, (c) Tp, (d) Number of catchments with NSE > 0, and (e) the difference in R<sup>2</sup>.

### 5.3. The influence of donor catchment quantity on machine-learning parameter regionalization

The number of donor catchments used in machine learning-based parameter



465 regionalization methods is a critical factor influencing the accuracy and robustness of  
466 hydrological predictions in ungauged catchments (Gauch et al., 2021; Song et al., 2022;  
467 Zhang et al., 2022). In this study, we investigated the influence of donor catchment  
468 quantity (ranging from 20 to 80) on the flood prediction performance of the two best-  
469 performing parameter regionalization methods (GBM4-KNN3 and GBM-KNN-ERT)  
470 across the 80 mountainous catchments (Fig 11). To systematically investigate the  
471 influence of donor catchment quantity on parameter regionalization, two distinct  
472 sampling strategies were employed across the 80 mountainous catchments. In Mode 1  
473 (selection of donor catchments based on decreasing NSE), a non-monotonic  
474 relationship between donor catchment quantity and regionalization performance was  
475 observed, indicating that simply increasing the number of donor catchments does not  
476 guarantee improved model performance. Specifically, in Mode 1, regionalization  
477 performance exhibited a significant decrease when the number of donor catchments  
478 exceeded 40 (particularly within the 40-60 range, and below 70 for GBM4-KNN3) (Fig.  
479 11a-c). This performance decline likely arises from the increasing dissimilarity in  
480 hydrological behavior between the added donor catchments and the target catchment as  
481 the donor pool expands, potentially introducing irrelevant or misleading information  
482 into the regionalization process (Gauch et al., 2021; Zhang et al., 2022). However, for  
483 the GBM-KNN-ERT method in Mode 1, regionalization performance tended to  
484 stabilize when the number of donor catchments exceeded 70, suggesting a potential  
485 saturation point beyond which additional donor catchments contribute little to  
486 improving model accuracy. In contrast, Mode 2 (random selection of donor catchments)



487 demonstrated a consistent improvement in regionalization performance for both NSE  
488 and  $T_p$  as the number of donor catchments increased (Fig. 11d-f). However, it's  
489 important to acknowledge that the potential for bias may also increase with the  
490 inclusion of more randomly selected donor catchments, potentially leading to  
491 overfitting or reduced generalizability. Notably, under both modes, the GBM-KNN-  
492 ERT method consistently exhibited significantly greater performance stability  
493 compared to the simpler combined strategy, GBM4-KNN3. This enhanced robustness  
494 likely arises from its more effective suppression of data heterogeneity and noise  
495 interference, indicating that more complex ensemble methods possess a greater  
496 capacity to balance the benefits of increased data quantity with the potential drawbacks  
497 of reduced data quality.

498

499

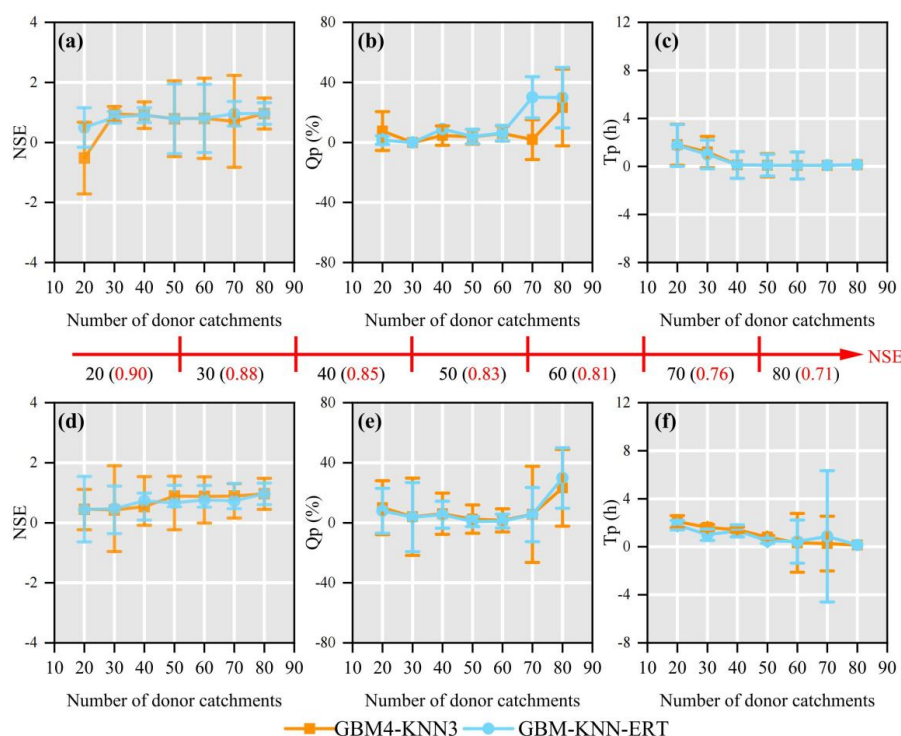


**Fig. 11.** Performance comparison of two donor catchment selection methods for parameter regionalization as a function of donor catchment quantity. Model 1 (a-c) selects donor catchments in order of decreasing NSE, while Model 2 (d-f) selects them randomly. Flood prediction accuracy is assessed using NSE, Qp, and Tp.

#### 5.4. The impact of climate change on parameter regionalization methods

The hydrological cycle within catchments is fundamentally governed by complex interactions between climate and environmental factors. The Intergovernmental Panel on Climate Change (IPCC) has consistently documented a continuous and accelerating transition in global climatic patterns, characterized by increased variability and extreme events (Pachauri et al., 2014). Consequently, future flood predictions derived from parameter regionalization methods are expected to exhibit increased uncertainty and variability, highlighting the substantial influence of climate change on the reliability and precision of flood predictions in ungauged mountainous catchments (Yang et al.,

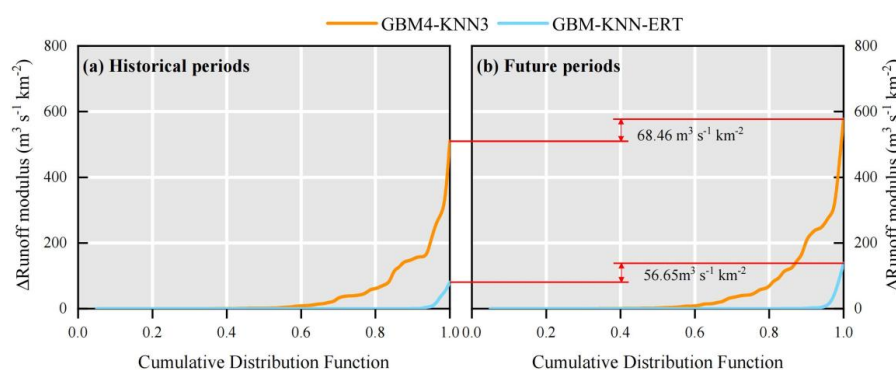


2019). Therefore, the stability and robustness of parameter regionalization methods under changing climatic conditions are paramount for their practical application in long-term flood risk assessment and management. To quantitatively assess the impact of climate change on the performance of the parameter regionalization methods, cumulative distribution functions (CDFs) were employed to illustrate the discrepancies between the parameter regionalization simulations and the reference simulations (derived from calibrated model parameters) across the historical (1901-2021) and projected future (2021-2100) periods for the 80 catchments (Fig 12). A comparative analysis of Fig. 12a and 12b reveals a clear amplification of the absolute differences in predicted flood peaks (quantified as the error in runoff modulus) between the two parameter regionalization methods and the reference Top-SSF model simulations during the transition from the historical period to the projected future period. Specifically, the maximum error in runoff modulus for the GBM4-KNN3 method increased by 67.26 m<sup>3</sup> s<sup>-1</sup> km<sup>-2</sup> from the historical period to the projected future period, while the equivalent maximum error for the GBM-KNN-ERT method increased by a smaller margin of 57.75 m<sup>3</sup> s<sup>-1</sup> km<sup>-2</sup> over the same period. These results underscore the increased sensitivity of parameter regionalization methods to changing climatic forcing conditions. However, they also provide compelling evidence that the GBM-KNN-ERT method exhibits superior stability and resilience under climate change, demonstrating its potential for more reliable long-term flood risk assessment in ungauged mountainous regions.

Exploring the effects of climate change on parameter regionalization methods



536 provides valuable insights for advancing flood prediction research in PUBs.  
537 Additionally, the combination of multiple machine learning methods, as demonstrated  
538 by the GBM-KNN-ERT method, shows increased stability under climate change,  
539 offering promising directions for future development of parameter regionalization  
540 methods.



541  
542 **Fig.12.** Comparison of flood peak runoff modulus between parameter regionalization and  
543 calibrated Top-SSF model results, showing cumulative distribution functions (CDFs) of  
544 absolute differences for 80 catchments during (a) historical and (b) future periods.

545

## 546 5.5. Uncertainty and limitation

547 The uncertainty in parameter regionalization within this study primarily originated  
548 from the hydrological model and the parameter regionalization methods. Although the  
549 Top-SSF model demonstrated satisfactory performance in flood prediction across the  
550 study catchments, inherent uncertainties associated with model parameters remained.  
551 To mitigate these uncertainties and enhance the reliability of the hydrological model,  
552 we employed the SCE-UA algorithm for parameter optimization and conducted  
553 comprehensive sensitivity analyses to identify and focus on the most influential  
554 parameters. The training data used in the machine learning-based parameter





555 regionalization methods, derived from the donor catchments, are susceptible to various  
556 sources of error, including noise, labeling inconsistencies, and missing values, all of  
557 which can contribute to increased estimation uncertainty (Mosavi et al., 2018; Xu et al.,  
558 2021).

559 Furthermore, the inherent stochasticity present in certain machine learning  
560 methods, such as ERT, can lead to outcome variations across different algorithm  
561 iterations, potentially influencing the stability and reproducibility of the results  
562 (Breiman, 2001; Geurts et al., 2006). To address the potential for overfitting and to  
563 obtain a more robust assessment of model performance, we employed K-fold cross-  
564 validation, a widely used technique that partitions the data into K subsets and iteratively  
565 evaluates model performance across different folds. This approach maximizes data  
566 utilization, improves the reliability of model performance evaluation by averaging  
567 results across multiple folds, and reduces the sensitivity to specific data partitioning  
568 schemes, thereby minimizing the overall uncertainty associated with the parameter  
569 regionalization methods. For hyperparameter tuning, we utilized the  
570 RandomizedSearchCV approach implemented in Python (Bergstra and Bengio, 2012).  
571 This method involves random sampling from a predefined hyperparameter space to  
572 identify the optimal hyperparameter combination for each machine learning method,  
573 thereby minimizing the potential for overfitting and improving the generalization  
574 performance of the models. The RandomizedSearchCV approach allows for a more  
575 comprehensive exploration of the hyperparameter space compared to grid search  
576 methods, even with a limited number of search iterations, and provides multiple



577 performance evaluations for a diverse range of model configurations. This random  
578 sampling strategy mitigates the uncertainty arising from fixed partitioning or manual  
579 parameter selection, ultimately enhancing the model's stability and its ability to  
580 generalize to unseen data (Bergstra and Bengio, 2012). During the assessment of  
581 parameter regionalization methods performance, the results were compared with the  
582 Top-SSF model simulation results (estimated model parameters and simulated flood  
583 process) rather than directly with measured flood data. Consequently, uncertainties  
584 related to the parameter regionalization methods may be significantly reduced.

## 585 **6. Conclusions**

586 This study introduces a novel multi-machine learning ensemble method (GBM-  
587 KNN-ERT) to enhance model parameter transferability and improve flood prediction  
588 in ungauged mountainous catchments. The proposed GBM-KNN-ERT method  
589 demonstrated a substantial advancement in both flood prediction accuracy and model  
590 robustness, achieving exceptional performance with 90% of ungauged catchments  
591 exhibiting a NSE exceeding 0.9, a significant 67.44% improvement compared to  
592 traditional single machine learning methods. Importantly, the GBM-KNN-ERT method  
593 exhibited remarkable stability under simulated climate change, thereby highlighting its  
594 potential for reliable application in non-stationary hydrological environments.  
595 Furthermore, the method demonstrated notable adaptability to varying donor-  
596 catchment configurations, achieving an optimal balance between predictive accuracy  
597 and computational efficiency with a relatively limited set of 20–40 high-quality donor  
598 catchments (NSE >0.85). By integrating the diverse strengths of multiple machine



599 learning with hydrological model, the proposed methodology significantly advances  
600 the field of flood prediction in ungauged catchments, offering a reliable tool for water  
601 resource management and flood disaster mitigation.

## 602 **Acknowledgements**

603 This research was supported by the National Natural Science Foundation of China  
604 (42330508 and 42271038) and the National Key Research and Development Program  
605 of China (2022FY100205).

## 606 **Competing interests**

607 The authors declare that they have no known competing financial interests or personal  
608 relationships that could have appeared to influence the work reported in this paper.

## 609 **Author contributions**

610 In this study, K L, G W, and J G were responsible for the conceptualization of the  
611 research. Data curation was carried out by K L, L G, and X S, while formal analysis  
612 was performed by K L, J G, and J M. The methodology was developed by K L, L G, P  
613 H, and J L. Project administration was overseen by G W and J G. K L took the lead in  
614 writing the original draft, and the writing, review, and editing process involved  
615 contributions from K L, G W, J L, P H, J M, X Z, and J G.

## 616 **Code and data availability**

617 The code used in this study is available upon request from the authors. The  
618 meteorological, soil characteristics, and topography datasets are publicly accessible  
619 online, as detailed in Table 1. The hourly flood data for the 80 catchments were sourced  
620 from China's Hydrological Yearbook. These data are not publicly available due to



621 governmental restrictions but can be accessed by contacting the corresponding author  
622 for further information.

## 623 **References**

- 624 Arsenault, R., Breton-Dufour, M., Poulin, A., Dallaire, G., Romero-Lopez, R. (2019).  
625 Streamflow prediction in ungauged basins: analysis of regionalization methods  
626 in a hydrologically heterogeneous region of Mexico. *Hydrological Sciences*  
627 *Journal*, 64(11): 1297-1311. <https://doi.org/10.1080/02626667.2019.1639716>  
628 Arsenault, R., Martel, J., Mai, J. (2022). Continuous streamflow prediction in ungauged  
629 basins: Long Short-Term Memory Neural Networks clearly outperform  
630 hydrological models. *Hydrol. Earth Syst. Sci.*: 1-29.  
631 <https://doi.org/10.5194/hess-27-139-2023>  
632 Bellman, R.E. (1961). On the reduction of dimensionality for classes of dynamic  
633 programming processes. RAND Corp., Santa Monica, Calif., Paper P-2243.  
634 Bergstra, J., Bengio, Y. (2012). Random search for hyper-parameter optimization.  
635 *Journal of machine learning research*, 13(2).  
636 Beven, K.J., Kirkby, M.J., Freer, J.E., Lamb, R. (2021). A history of TOPMODEL.  
637 *Hydrology and Earth System Sciences*, 25(2): 527-549.  
638 <https://doi.org/10.5194/hess-25-527-2021>  
639 Bishop, C.M., Nasrabadi, N.M., (2006). Pattern recognition and machine learning  
640 (information science and statistics). New York: Springer - Verlag.  
641 Breiman, L. (2001). Random forests. *Machine learning*, 45: 5-32.  
642 Cheng, Q., Gao, L., Zuo, X., Zhong, F. (2019). Statistical analyses of spatial and  
643 temporal variabilities in total, daytime, and nighttime precipitation indices and  
644 of extreme dry/wet association with large-scale circulations of Southwest China,  
645 1961–2016. *Atmospheric research*, 219: 166-182.  
646 <https://doi.org/10.1109/ACCESS.2018.2886549>  
647 Choi, J., Kim, U., Kim, S. (2023). Ecohydrologic model with satellite-based data for  
648 predicting streamflow in ungauged basins. *Science of The Total Environment*,  
649 903: 166617. <https://doi.org/10.1016/j.scitotenv.2023.166617>  
650 Dai, Y., Shangguan, W., Duan, Q., Liu, B., Fu, S., Niu, G. (2013). Development of a  
651 China dataset of soil hydraulic parameters using pedotransfer functions for land  
652 surface modeling. *Journal of Hydrometeorology*, 14(3): 869-887.  
653 <https://doi.org/10.1175/JHM-D-12-0149.1>  
654 Dakhlaoui, H., Bargaoui, Z., Bárdossy, A. (2012). Toward a more efficient calibration  
655 schema for HBV rainfall–runoff model. *Journal of Hydrology*, 444: 161-179.  
656 <https://doi.org/10.1016/j.jhydrol.2012.04.015>  
657 Ding, Y., Peng, S. (2020). Spatiotemporal trends and attribution of drought across China  
658 from 1901–2100. *Sustainability*, 12(2): 477.  
659 <https://doi.org/10.3390/su12020477>



- 660 Duan, Q., Sorooshian, S.Gupta, V.K. (1994). Optimal use of the SCE-UA global  
661 optimization method for calibrating watershed models. *Journal of Hydrology*,  
662 158(3): 265-284. [https://doi.org/10.1016/0022-1694\(94\)90057-4](https://doi.org/10.1016/0022-1694(94)90057-4)
- 663 Friedman, J.H. (2002). Stochastic gradient boosting. *Computational statistics & data*  
664 *analysis*, 38(4): 367-378. [https://doi.org/10.1016/S0167-9473\(01\)00065-2](https://doi.org/10.1016/S0167-9473(01)00065-2)
- 665 Gan, B., Liu, X., Yang, X., Wang, X.Zhou, J. (2018). The impact of human activities on  
666 the occurrence of mountain flood hazards: lessons from the 17 August 2015  
667 flash flood/debris flow event in Xuyong County, south-western China.  
668 *Geomatics, Natural Hazards and Risk*, 9(1): 816-840.  
669 <https://doi.org/10.1080/19475705.2018.1480539>
- 670 Gao, J., Kirkby, M.Holden, J. (2018). The effect of interactions between rainfall  
671 patterns and land-cover change on flood peaks in upland peatlands. *Journal of*  
672 *Hydrology*, 567: 546-559. <https://doi.org/10.1016/j.jhydrol.2018.10.039>
- 673 Garambois, P.A., Roux, H., Larnier, K., Labat, D.Dartus, D. (2015). Parameter  
674 regionalization for a process-oriented distributed model dedicated to flash  
675 floods. *Journal of Hydrology*, 525: 383-399.  
676 <https://doi.org/10.1016/j.jhydrol.2015.03.052>
- 677 Gauch, M., Mai, J.Lin, J. (2021). The proper care and feeding of CAMELS: How  
678 limited training data affects streamflow prediction. *Environmental Modelling &*  
679 *Software*, 135: 104926. <https://doi.org/10.1016/j.envsoft.2020.104926>
- 680 Geurts, P., Ernst, D.Wehenkel, L. (2006). Extremely randomized trees. *Machine*  
681 *Learning*, 63(1): 3-42. <https://doi.org/10.1007/s10994-006-6226-1>
- 682 Golian, S., Murphy, C.Meresa, H. (2021). Regionalization of hydrological models for  
683 flow estimation in ungauged catchments in Ireland. *Journal of Hydrology:*  
684 *Regional Studies*, 36: 100859. <https://doi.org/10.1016/j.ejrh.2021.100859>
- 685 Guo, L., Huang, K., Wang, G.Lin, S. (2022). Development and evaluation of  
686 temperature-induced variable source area runoff generation model. *Journal of*  
687 *Hydrology*, 610: 127894. <https://doi.org/10.1016/j.jhydrol.2022.127894>
- 688 Guo, Y., Zhang, Y., Zhang, L.Wang, Z. (2021). Regionalization of hydrological  
689 modeling for predicting streamflow in ungauged catchments: A comprehensive  
690 review. *Wiley Interdisciplinary Reviews: Water*, 8(1): e1487.  
691 <https://doi.org/10.1002/wat2.1487>
- 692 Gupta, A.K., Chakroborty, S., Ghosh, S.K.Ganguly, S. (2023). A machine learning  
693 model for multi-class classification of quenched and partitioned steel  
694 microstructure type by the k-nearest neighbor algorithm. *Computational*  
695 *Materials Science*, 228: 112321.  
696 <https://doi.org/10.1016/j.commatsci.2023.112321>
- 697 Hastie, T., Tibshirani, R.Friedman, J., (2009). *The elements of statistical learning*.  
698 Citeseer.
- 699 Hersbach, H., Bell, B., Berrisford, P., Biavati, G., Horányi, A., Muñoz Sabater, J.,  
700 Nicolas, J., Peubey, C., Radu, R., Rozum, I., Schepers, D., Simmons, A., Soci,  
701 C., Dee, D.Thépaut, J.-N., (2023). ERA5 hourly data on single levels from 1940  
702 to present, Copernicus Climate Change Service (C3S) Climate Data Store



- 703 (CDS)[Dataset]. <https://doi.org/10.24381/cds.adbb2d47> (Accessed on 08-06-  
704 2023)
- 705 Hua, F., Wang, L., Fisher, B., Zheng, X., Wang, X., Douglas, W.Y., Tang, Y., Zhu,  
706 J.Wilcove, D.S. (2018). Tree plantations displacing native forests: The nature  
707 and drivers of apparent forest recovery on former croplands in Southwestern  
708 China from 2000 to 2015. *Biological Conservation*, 222: 113-124.  
709 <https://doi.org/10.1016/j.biocon.2018.03.034>
- 710 Jordan, M.I.Mitchell, T.M. (2015). Machine learning: Trends, perspectives, and  
711 prospects. *Science*, 349(6245): 255-260. <https://doi.org/10.1126/science.aaa841>
- 712 Jung, Y. (2018). Multiple predicting K-fold cross-validation for model selection.  
713 *Journal of Nonparametric Statistics*, 30(1): 197-215.  
714 <https://doi.org/10.1080/10485252.2017.1404598>
- 715 Kanishka, G.Eldho, T. (2017). Watershed classification using isomap technique and  
716 hydrometeorological attributes. *Journal of Hydrologic Engineering*, 22(10):  
717 04017040. [https://doi.org/10.1061/\(ASCE\)HE.1943-5584.0001562](https://doi.org/10.1061/(ASCE)HE.1943-5584.0001562)
- 718 Kratzert, F., Klotz, D., Herrnegger, M., Sampson, A.K., Hochreiter, S.Nearing, G.S.  
719 (2019). Toward improved predictions in ungauged basins: Exploiting the power  
720 of machine learning. *Water Resources Research*, 55(12): 11344-11354.  
721 <https://doi.org/10.1029/2019WR026065>
- 722 Lenhart, T., Eckhardt, K., Fohrer, N.Frede, H.G. (2002). Comparison of two different  
723 approaches of sensitivity analysis. *Physics and Chemistry of the Earth, Parts*  
724 *A/B/C*, 27(9): 645-654. [https://doi.org/10.1016/S1474-7065\(02\)00049-9](https://doi.org/10.1016/S1474-7065(02)00049-9)
- 725 Li, K., Wang, G., Gao, J., Guo, L., Li, J.Guan, M. (2024). The rainfall threshold of  
726 forest cover for regulating extreme floods in mountainous catchments. *Catena*,  
727 236: 107707. <https://doi.org/10.1016/j.catena.2023.107707>
- 728 Li, X., Khandelwal, A., Jia, X., Cutler, K., Ghosh, R., Renganathan, A., Xu, S., Tayal,  
729 K., Nieber, J.Duffy, C. (2022). Regionalization in a global hydrologic deep  
730 learning model: from physical descriptors to random vectors. *Water Resources*  
731 *Research*, 58(8): e2021WR031794. <https://doi.org/10.1029/2021WR031794>
- 732 Li, Z., Xu, X., Yu, B., Xu, C., Liu, M.Wang, K. (2016). Quantifying the impacts of  
733 climate and human activities on water and sediment discharge in a karst region  
734 of southwest China. *Journal of Hydrology*, 542: 836-849.  
735 <https://doi.org/10.1016/j.jhydrol.2016.09.049>
- 736 Liu, C., Guo, L., Ye, L., Zhang, S., Zhao, Y.Song, T. (2018). A review of advances in  
737 China's flash flood early-warning system. *Natural hazards*, 92: 619-634.  
738 <https://doi.org/10.1007/s11069-018-3173-7>
- 739 Luo, P., He, B., Takara, K., Xiong, Y.E., Nover, D., Duan, W.Fukushi, K. (2015).  
740 Historical assessment of Chinese and Japanese flood management policies and  
741 implications for managing future floods. *Environmental Science & Policy*, 48:  
742 265-277. <https://doi.org/10.1016/j.envsci.2014.12.015>
- 743 McMillan, H.K. (2021). A review of hydrologic signatures and their applications. *Wiley*  
744 *Interdisciplinary Reviews: Water*, 8(1): e1499.  
745 <https://doi.org/10.1002/wat2.1499>



- 746 Morel-Seytoux, H.J.Khanji, J. (1974). Derivation of an equation of infiltration. Water  
747 Resources Research, 10(4): 795-800.  
748 <https://doi.org/10.1029/WR010i004p00795>
- 749 Mosavi, A., Ozturk, P.Chau, K.w. (2018). Flood prediction using machine learning  
750 models: Literature review. Water, 10(11): 1536.  
751 <https://doi.org/10.3390/w10111536>
- 752 Nearing, G., Cohen, D., Dube, V., Gauch, M., Gilon, O., Harrigan, S., Hassidim, A.,  
753 Klotz, D., Kratzert, F., Metzger, A., Nevo, S., Pappenberger, F., Prudhomme, C.,  
754 Shalev, G., Shenzis, S., Tekalign, T.Y., Weitzner, D.Matias, Y. (2024). Global  
755 prediction of extreme floods in ungauged watersheds. Nature, 627(8004): 559-  
756 563. <https://doi.org/10.1038/s41586-024-07145-1>
- 757 Pachauri, R.K., Allen, M.R., Barros, V.R., Broome, J., Cramer, W., Christ, R., Church,  
758 J.A., Clarke, L., Dahe, Q.Dasgupta, P., (2014). Climate change 2014: synthesis  
759 report. Contribution of Working Groups I, II and III to the fifth assessment  
760 report of the Intergovernmental Panel on Climate Change.
- 761 Papageorgaki, I.Nalbantis, I. (2016). Classification of Drainage Basins Based on  
762 Readily Available Information. Water Resources Management, 30(15): 5559-  
763 5574. <https://doi.org/10.1007/s11269-016-1410-y>
- 764 Pugliese, A., Persiano, S., Bagli, S., Mazzoli, P., Parajka, J., Arheimer, B., Capell, R.,  
765 Montanari, A., Blöschl, G.Castellarin, A. (2018). A geostatistical data-  
766 assimilation technique for enhancing macro-scale rainfall-runoff simulations.  
767 Hydrology and Earth System Sciences, 22(9): 4633-4648.  
768 <https://doi.org/10.5194/hess-22-4633-2018>
- 769 Qi, W., Zhang, C., Fu, G.Zhou, H. (2016). Quantifying dynamic sensitivity of  
770 optimization algorithm parameters to improve hydrological model calibration.  
771 Journal of Hydrology, 533: 213-223.  
772 <https://doi.org/10.1016/j.jhydrol.2015.11.052>
- 773 Ragetti, S., Zhou, J., Wang, H., Liu, C.Guo, L. (2017). Modeling flash floods in  
774 ungauged mountain catchments of China: A decision tree learning approach for  
775 parameter regionalization. Journal of Hydrology, 555: 330-346.  
776 <https://doi.org/10.1016/j.jhydrol.2017.10.031>
- 777 Rockström, J., Gupta, J., Qin, D., Lade, S.J., Abrams, J.F., Andersen, L.S., Armstrong  
778 McKay, D.I., Bai, X., Bala, G., Bunn, S.E., Ciobanu, D., DeClerck, F., Ebi, K.,  
779 Gifford, L., Gordon, C., Hasan, S., Kanie, N., Lenton, T.M., Loriani, S.,  
780 Liverman, D.M., Mohamed, A., Nakicenovic, N., Obura, D., Ospina, D.,  
781 Prodani, K., Rammelt, C., Sakschewski, B., Scholtens, J., Stewart-Koster, B.,  
782 Tharammal, T., van Vuuren, D., Verburg, P.H., Winkelmann, R., Zimm, C.,  
783 Bennett, E.M., Bringezu, S., Broadgate, W., Green, P.A., Huang, L., Jacobson,  
784 L., Ndehedehe, C., Pedde, S., Rocha, J., Scheffer, M., Schulte-Uebbing, L., de  
785 Vries, W., Xiao, C., Xu, C., Xu, X., Zafra-Calvo, N.Zhang, X. (2023). Safe and  
786 just Earth system boundaries. Nature, 619(7968): 102-111.  
787 <https://doi.org/10.1038/s41586-023-06083-8>
- 788 Sain, S.R. (1996). The Nature of Statistical Learning Theory. Technometrics, 38(4):  
789 409-409. <https://doi.org/10.1080/00401706.1996.10484565>





- 790 Salmeron, R., García, C.García, J. (2018). Variance inflation factor and condition  
791 number in multiple linear regression. Journal of statistical computation and  
792 simulation, 88(12): 2365-2384.  
793 <https://doi.org/10.1080/00949655.2018.1463376>
- 794 Schoups, G., van de Giesen, N.C.Savenije, H.H.G. (2008). Model complexity control  
795 for hydrologic prediction. Water Resources Research, 44(12).  
796 <https://doi.org/10.1029/2008WR006836>
- 797 Shanguan, W., Dai, Y., Liu, B., Zhu, A., Duan, Q., Wu, L., Ji, D., Ye, A., Yuan,  
798 H.Zhang, Q. (2013). A China data set of soil properties for land surface  
799 modeling. Journal of Advances in Modeling Earth Systems, 5(2): 212-224.  
800 <https://doi.org/10.1002/jame.20026>
- 801 Song, Z., Xia, J., Wang, G., She, D., Hu, C.Hong, S. (2022). Regionalization of  
802 hydrological model parameters using gradient boosting machine. Hydrology  
803 and Earth System Sciences, 26(2): 505-524. [https://doi.org/10.5194/hess-26-](https://doi.org/10.5194/hess-26-505-2022)  
804 [505-2022](https://doi.org/10.5194/hess-26-505-2022)
- 805 Tang, S., Sun, F., Liu, W., Wang, H., Feng, Y.Li, Z. (2023). Optimal Postprocessing  
806 Strategies With LSTM for Global Streamflow Prediction in Ungauged Basins.  
807 Water Resources Research, 59(7): e2022WR034352.  
808 <https://doi.org/10.1029/2022WR034352>
- 809 Wainwright, J.Mulligan, M., (2013). Environmental modelling: finding simplicity in  
810 complexity. John Wiley & Sons.
- 811 Wani, O., Beckers, J.V.L., Weerts, A.H.Solomatine, D.P. (2017). Residual uncertainty  
812 estimation using instance-based learning with applications to hydrologic  
813 forecasting. Hydrol. Earth Syst. Sci., 21(8): 4021-4036.  
814 <https://doi.org/10.5194/hess-21-4021-2017>
- 815 Wu, H., Zhang, J., Bao, Z., Wang, G., Wang, W., Yang, Y.Wang, J. (2022). Runoff  
816 modeling in ungauged catchments using machine learning algorithm-based  
817 model parameters regionalization methodology. Engineering.  
818 <https://doi.org/10.1016/j.eng.2021.12.014>
- 819 Xu, Q., Chen, J., Peart, M.R., Ng, C.-N., Hau, B.C.H.Law, W.W.Y. (2018). Exploration  
820 of severities of rainfall and runoff extremes in ungauged catchments: A case  
821 study of Lai Chi Wo in Hong Kong, China. Science of The Total Environment,  
822 634: 640-649. <https://doi.org/10.1016/j.scitotenv.2018.04.024>
- 823 Xu, T.Liang, F. (2021). Machine learning for hydrologic sciences: An introductory  
824 overview. Wiley Interdisciplinary Reviews: Water, 8(5).  
825 <https://doi.org/10.1002/wat2.1533>
- 826 Yang, X., Magnusson, J., Rizzi, J.Xu, C.-Y. (2018). Runoff prediction in ungauged  
827 catchments in Norway: comparison of regionalization approaches. Hydrology  
828 Research, 49(2): 487-505. <https://doi.org/10.2166/nh.2017.071>
- 829 Yang, X., Magnusson, J.Xu, C.Y. (2019). Transferability of regionalization methods  
830 under changing climate. Journal of Hydrology, 568: 67-81.  
831 <https://doi.org/10.1016/j.jhydrol.2018.10.030>
- 832 Zhai, X., Guo, L., Liu, R.Zhang, Y. (2018). Rainfall threshold determination for flash  
833 flood warning in mountainous catchments with consideration of antecedent soil





- 834 moisture and rainfall pattern. *Natural Hazards*, 94: 605-625.  
835 <https://doi.org/10.1007/s11069-018-3404-y>  
836 Zhang, B., Ouyang, C., Cui, P., Xu, Q., Wang, D., Zhang, F., Li, Z., Fan, L., Lovati, M.,  
837 Liu, Y. Zhang, Q. (2024). Deep learning for cross-region streamflow and flood  
838 forecasting at a global scale. *The Innovation*, 5(3).  
839 <https://doi.org/10.1016/j.xinn.2024.100617>  
840 Zhang, Y., Chiew, F.H., Li, M. Post, D. (2018). Predicting runoff signatures using  
841 regression and hydrological modeling approaches. *Water Resources Research*,  
842 54(10): 7859-7878. <https://doi.org/10.1029/2018WR023325>  
843 Zhang, Y., Chiew, F.H., Liu, C., Tang, Q., Xia, J., Tian, J., Kong, D. Li, C. (2020). Can  
844 remotely sensed actual evapotranspiration facilitate hydrological prediction in  
845 ungauged regions without runoff calibration? *Water Resources Research*, 56(1):  
846 e2019WR026236. <https://doi.org/10.1029/2019WR026236>  
847 Zhang, Y., Ragettli, S., Molnar, P., Fink, O. Peleg, N. (2022). Generalization of an  
848 Encoder-Decoder LSTM model for flood prediction in ungauged catchments.  
849 *Journal of Hydrology*, 614: 128577.  
850 <https://doi.org/10.1016/j.jhydrol.2022.128577>  
851 Zounemat-Kermani, M., Batelaan, O., Fadaee, M. Hinkelmann, R. (2021). Ensemble  
852 machine learning paradigms in hydrology: A review. *Journal of Hydrology*, 598:  
853 126266. <https://doi.org/10.1016/j.jhydrol.2021.126266>

854